TURBULENCE DISTORTION EFFECTS FOR LEADING-EDGE NOISE PREDICTION

Fernanda Leticia dos Santos, Kees Venner and Leandro Dantas de Santana
University of Twente, Enschede, The Netherlands
e-mail: f.l.dossantos@utwente.nl

Leading-edge noise is the dominant noise source for applications such as propellers and fans. Amiet's leading-edge noise model is widely used to predict this noise source during the design for these applications. However, Amiet's model is based on an infinitely thin flat plate assumption, not accounting for real airfoil geometric effects, resulting in inaccurate noise estimation for airfoils. The leading-edge noise is mainly affected by the turbulence distortion caused by the airfoil blocking effect due to its finite thickness. This paper discusses the turbulence distortion caused by different airfoil geometries and how to account for turbulence distortion in Amiet's model. Experiments were performed in the Aeroacoustic Wind Tunnel of the University of Twente. The inflow turbulence was generated by a rod. The airfoil geometries tested were NACA0008, NACA0012, and NACA0018. The inflow turbulence distortion was measured in the vicinity of the airfoil leading edge by hot-wire anemometry. In addition, the noise radiated by rod-airfoil interaction was measured and compared with Amiet's noise prediction model. The results show that the velocity fluctuations and turbulence length scale at the stagnation line decreased in the vicinity of the airfoil leading edge. Amiet's model overestimates the leading-edge noise for high frequencies. The predicted leading-edge noise agrees well with the measurements when the turbulence distortion is taken into account in the turbulence spectrum formulation and in the input values of the root-mean-square of the velocity fluctuations and the turbulence length scale. Thus, Amiet's leading-edge noise prediction model can be corrected to account for the turbulence distortion. Keywords: leading-edge noise, turbulence distortion

1. Introduction

Aeroacoustic noise pollution impacts the well-being of people and animal life. The societal need to reduce this noise motivated the creation of stringent regulations that impose sound limits for this noise source. Leading-edge (LE) noise is an aeroacoustic noise mechanism that is dominant for applications exposed to turbulent inflow [1], e.g., propellers and fans. LE noise is generated by the interaction of the unsteady turbulent inflow with the LE of a foil [2]. Amiet's LE noise prediction model [3] is commonly used for the design and optimization of these applications due to its computational simplicity and short

turnaround time. However, Amiet's model is based on an infinitely thin flat plate geometry; i.e., it does not account for geometric airfoil parameters, e.g., thickness, camber, and angle of attack. These parameters influence the radiated noise [4, 5, 6], with the airfoil thickness and LE radius impacting the LE far-field noise the most [4, 5].

Moreau and Roger [5] measured the far-field noise generated by different airfoil geometries and compared the measurements with Amiet's model. They observed that the model overestimates the LE far-field noise for high frequencies. They attributed this to the finite airfoil thickness. This behavior was also observed by Oerlemans and Migliore [6]. According to Gill et al. [7], the mismatch between the predicted and the measured noise at high frequencies is due to the inflow turbulence distortion caused by the velocity gradients in the LE stagnation region. Moreau and Roger [5] proposed a correction to the inflow velocity spectrum to account for the inflow turbulence distortion. The corrected spectrum was derived using the rapid distortion theory (RDT) [8]. Moreau and Roger [5] showed that using the corrected velocity spectrum, the far-field noise prediction for high frequencies agreed better with the measured noise. In their study, the inflow turbulence characteristics, i.e., the root-mean-square of the velocity fluctuations and the integral length scale, which were used as input for the noise prediction model, were measured at the LE location with the airfoil removed. This approach is common in LE noise studies, see also Devenport et al. [4]. Using a similar methodology as Moreau and Roger [5], de Santana et al. [9] formulated a semi-empirical RDT-based velocity spectrum to predict the turbulence distortion occurring at the airfoil LE. Dos Santos et al. [10] investigated the turbulence distortion effects in the LE vicinity of a NACA 0008 airfoil. Also, they described how to account for the turbulence distortion in Amiet's model. They showed that the experimental and predicted LE noise agreed reasonably well if the turbulence distortion is considered in the turbulence spectrum formulation and the turbulence input parameters for Amiet's model. From these studies, it is clear that turbulence distortion is an important effect that must be considered in noise prediction. However, a better understanding of the turbulence distortion effects and the capability of Amiet's model to account for this effect for several airfoil geometries still require further investigation.

This paper aims to experimentally study the turbulence distortion caused by different airfoil geometries to improve Amiet's LE noise prediction model. The paper is organized as follows. Section 2 describes the airfoil models used and the measurements performed. Section 3 discusses the turbulence characteristics in the LE vicinity of the different airfoils. Section 4 compares the measured and predicted LE noise for different cases where the turbulence distortion is and is not taken into account. Section 5 states the main conclusions of this study.

2. Experimental methodology

2.1 Wind tunnel and airfoil models

Experiments were conducted in the UTwente AeroAcoustic Wind Tunnel, an open-jet, closed-circuit facility [11]. The inflow turbulence was generated by a rod of 40 mm diameter, positioned approximately 1 m upstream of the airfoil LE. The measurements were performed for free-stream velocities (U) from 20 to 40 m/s. However, only experiments at 30 m/s are discussed in this paper for brevity.

Three airfoils were tested: NACA 0008, NACA 0012, and NACA 0018. These geometries were chosen because they have different thicknesses and LE radii. The geometric parameters for the airfoils are listed in Table 1, where c is the chord length, d is the span length, r_{LE} is the LE radius, and t is the maximum thickness. The angle of attack was zero for all experiments. The coordinate system considers the downstream direction as the x direction, the spanwise direction as the y direction, and the normal-to-the-surface direction as the z direction, with the origin at the LE position and midspan, see Fig. 1.

Table 1: Geometric parameters of the airfoils used in this research.

Airfoil	c [mm]	d [mm]	r_{LE} [mm]	t [mm]
NACA 0008	300	700	2.1	24
NACA 0012	200	700	3.2	24
NACA 0018	200	700	7.1	36

2.2 Hot-wire measurements

The inflow turbulence was evaluated using hot-wire anemometry, see Fig. 1(a), for the cases with and without the airfoil present in the flow. A single-wire probe (Dantec Dynamics 55P15) measured the velocity in the x direction (u). The hot-wire data was acquired by the Dantec StreamLine Pro CTA system and the Dantec StreamWare software in combination with the National Instruments 9215 A/D converter. The data was recorded for 30 s with a sampling frequency of 65,536 Hz and an anti-aliasing low-pass filter with a cutoff frequency of 30 kHz. A high-pass filter with a cutoff frequency of 5 Hz was used during the post-processing to eliminate the effect of the flow buffeting instability present in an open test section wind tunnel [12] because this effect has a direct influence on the length scale calculation. The velocity was measured for locations upstream and in the vicinity of the airfoil LE, reaching distances up to $x/r_{LE} = -1.8$. Measurements closer to the LE were not possible due to the physical constraints imposed by the hot-wire probe. These measurements were conducted in the stagnation line at midspan. The velocity was also measured without the airfoil in the flow at the LE location.

2.3 Far-field noise measurements

A microphone phased array consisting of 62 microphones (GRAS 40PH) was used to localize and quantify the LE noise, see Fig. 1(b). The sensitivity of each microphone was calibrated using a piston-phone (GRAS 42AG Multifunction Sound Calibrator). The distance between the microphone and the airfoil was 1.5 m and the center of the array was aligned with the airfoil center. Data was acquired at a sampling frequency of 65,536 Hz using PXIe-4499 Sound and Vibration modules installed in a NI PXIe-1073 chassis. The acquisition time was 30 seconds.

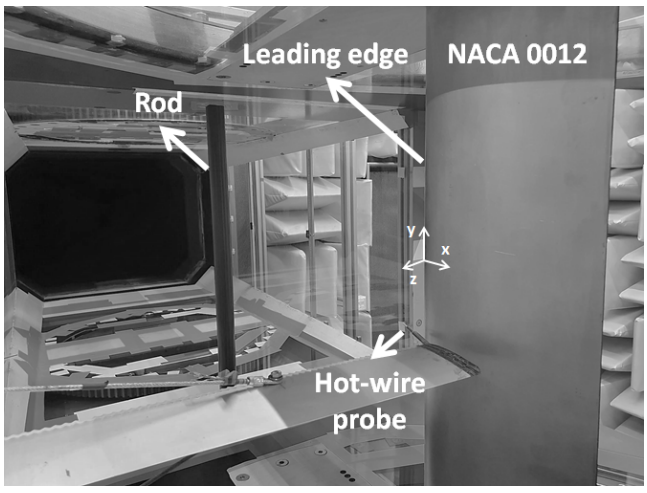

(a) Hot-wire setup

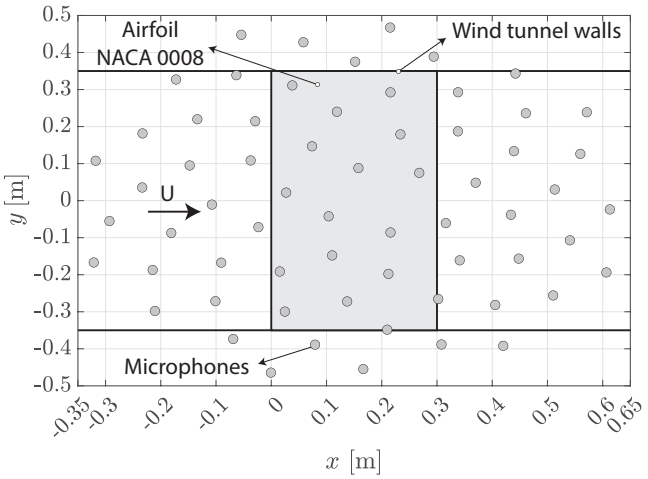

(b) Schematic view of the microphone locations in the array and position relative to the airfoil

Figure 1: Experimental setups.

The noise localization and quantification were done using an in-house beamforming code. The cross-spectral matrix (CSM) was estimated using Welch's method. The data was averaged using blocks of 8192 samples (125 ms) and windowed by a Hanning windowing function with 50% overlap, resulting in a frequency resolution of 8 Hz. Conventional beamforming in the frequency domain was performed on a searching grid $x/c = [-2, 3]$ and $z/d = [-0.71, 0.71]$ in the plane composed by the airfoil chord-span lines. The grid resolution was 30 mm. The LE noise radiated by the airfoils was isolated with the source power integration (SPI) technique [13]. The region of integration (ROI) was $x/c = [-0.5, 0.5]$ and $z/d = [-0.3, 0.3]$. The power spectral density (PSD) from the SPI is given at the array center.

3. Turbulence characteristics in the vicinity of the airfoil leading edge

In this section, the hot-wire measurements are discussed. NTD and TD stand for No Turbulence Distortion and Turbulence Distortion, respectively. For the NTD case, the airfoil was not present in the flow. Hence, the turbulence was not distorted by the mean flow caused by the airfoil. For the TD case, the airfoil was in the flow. Thus, the turbulence was distorted by the velocity gradients in the LE stagnation region [7].

Figure 2 shows the behavior of the turbulence longitudinal length scale (Λ_f) and the root-mean-square of the downstream velocity fluctuations (u_{rms}) for locations close to the airfoil LE. Also, the values of Λ_f and u_{rms} at the LE position for the NTD case are included ("No Airfoil - NTD"). Λ_f was calculated as proposed by Hinze [14]. The x axes are nondimensionalized by the LE radius because r_{LE} is the relevant dimension for the turbulence distortion in the vicinity of an airfoil LE [15].

Figure 2 shows that Λ_f rapidly decreases as the airfoil LE is approached ($x/r_{\mathrm{LE}} > -10$), which is due to the airfoil blockage effect. This observation indicates that the turbulence is distorted in the vicinity of the airfoil LE. The distortion occurs due to the velocity gradients in the stagnation region, as discussed by Gill et al. [7]. For $x/r_{\mathrm{LE}} < -10$, Λ_f is not affect by the airfoil presence, reaching its free-stream value. For u_{rms}, two phenomena are observed: (1) energy dissipation as the turbulence is convected downstream, as discussed by dos Santos et al. [16], and (2) airfoil blockage effects. The rapid decay of u_{rms} for downstream positions $-30 < x/r_{\mathrm{LE}} < -5$ is because energy is dissipated as the turbulent structures are convected in the downstream direction. For positions $x/r_{\mathrm{LE}} > -5$, the blockage effect caused by the airfoil becomes the dominant phenomenon, inducing a rapid decay of the velocity

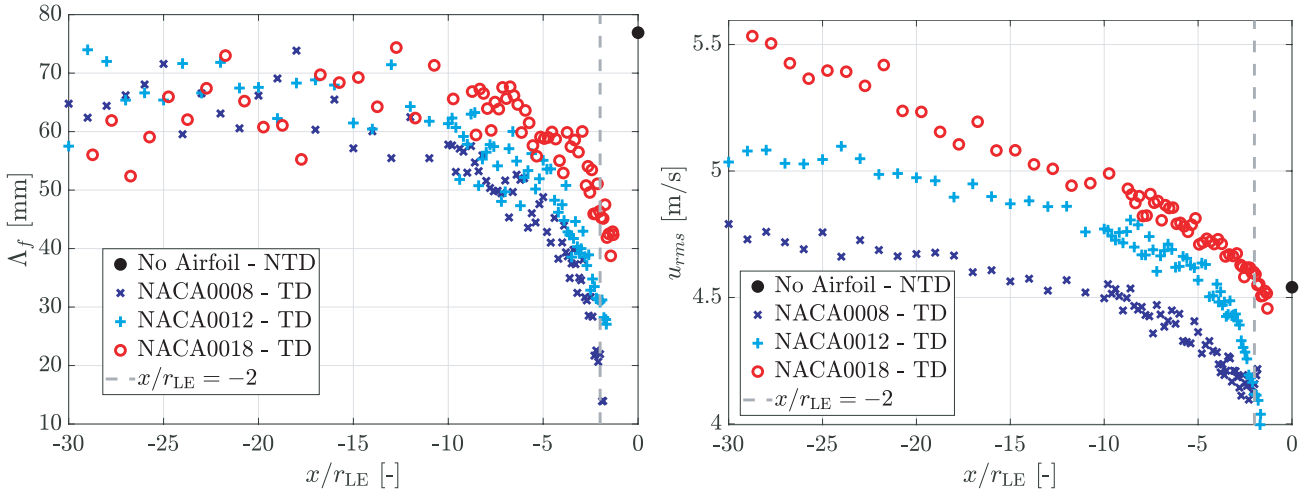

Figure 2: Longitudinal length scale and root-mean-square of the velocity fluctuations in the vicinity of the airfoil LE. Black circle at $x/r_{\mathrm{LE}} = 0$ refers to the NTD case.

fluctuations. This behavior can be seen more clearly by comparing the u_{rms} value at $x/r_{\mathrm{LE}} = -2$ for the NACA 0008 and NACA 0012 to the u_{rms} value at $x/r_{\mathrm{LE}} = 0$ for the "No Airfoil - NTD" case. However, for the NACA 0018, the u_{rms} value at $x/r_{\mathrm{LE}} = -2$ is similar to the u_{rms} value at $x/r_{\mathrm{LE}} = 0$ for the "No Airfoil - NTD" case. These observations show that for a thicker airfoil, in this case NACA 0018, the u_{rms} decay due to the airfoil blockage effect is concentrated for positions $x/r_{\mathrm{LE}} > -2$. Furthermore, Λ_f and u_{rms} at $x/r_{\mathrm{LE}} = -2$ decrease as the airfoil LE radius and thickness decrease. This behavior has a direct impact on the LE noise generated by these airfoils, which will be discussed in Section 4. Even though some airfoils have a different chord length, the chord length should not play a role in the turbulence distortion. The distortion is a local phenomenon localized in the vicinity of the airfoil LE, with the LE radius and the thickness being the relevant dimensions.

4. Leading-edge far-field noise measurement and prediction

4.1 Noise prediction model

Amiet [3] proposed a semi-analytical model for predicting the far-field noise generated by the interaction of a turbulent stream with a flat plate of infinitely small thickness. The two-sided PSD of the far-field noise generated by a flat plate of chord c and span d considering an observer in the plane $y = 0$ is given as [3, pp. 411]:

$$S_{pp}^{Amiet}(x_o, y_o = 0, z_o, \omega) = \left(\frac{\omega z_o \rho (c/2)}{c_o \sigma^2}\right)^2 \pi U (d/2) \left|\mathscr{L}(\vec{x}, K_x, 0)\right|^2 \Phi_{ww}(K_x, 0) \tag{1}$$

where $\vec{x} = (x_0,y_0,z_0)$ is the observer location, $\omega = 2\pi f$ is the angular frequency, f is the ordinary frequency, ρ is the fluid density, c_0 is the speed of sound, $\sigma^2 = x_o^2 + (1 - M^2)(y_o^2 + z_o^2)$, M is the Mach number, $\mathscr{L}$ is the aeroacoustic transfer function (determined from de Santana [17, pp. 155,166,168]), Φ_{ww} is the inflow turbulence spectrum, and $K_x = \omega/U$. The coordinate system is the same as the one presented in Sec. 2. However, the origin is located at mid-chord and midspan of the airfoil surface for the noise prediction model. Equation 1 is converted to a one-sided PSD (factor of 2) with a dependence on f instead of ω (factor of 2π) by:

$$G_{pp}^{Amiet}(x_o, y_o = 0, z_o, f) = (2 \times 2\pi) S_{pp}(x_o, y_o = 0, z_o, \omega) \tag{2}$$

The far-field noise can be calculated from the inflow turbulence spectrum, usually represented by the von Kármán turbulence spectrum [2, pp. 191]:

$$\Phi_{ww}^{\mathrm{vK}}(k_x, k_y) = \frac{4}{9\pi} \frac{u_{rms}^2}{k_e^2} \frac{(k_x/k_e)^2 + (k_y/k_e)^2}{[1 + (k_x/k_e)^2 + (k_y/k_e)^2]^{7/3}} \tag{3}$$

where $k_e = (\sqrt{\pi}/\Lambda_f)(\Gamma(5/6)/\Gamma(1/3))$ is the wavenumber scale of the largest eddies, Γ is the gamma function, k_x and k_y are the wavenumber in the x and y directions, respectively.

To account for the turbulence distortion, de Santana et al. [9] proposed a modification to the energy turbulence spectrum based on the asymptotic results of the rapid distortion theory (RDT) [8], which is given as [9, pp. 353]:

$$\Phi_{ww}^{\mathrm{RDT}}(k_x, k_y) = \frac{91}{36\pi} \frac{u_{rms}^2}{k_e^2} \frac{(k_x/k_e)^2 + (k_y/k_e)^2}{[1 + (k_x/k_e)^2 + (k_y/k_e)^2]^{19/6}} \tag{4}$$

In this study, both spectra (Eqs. 3 and 4) were used as input for Amiet's noise prediction model (Eq. 1).

4.2 Comparison between the measured and predicted noise

Figure 3 shows the measured and predicted LE noise for an observer localized at the microphone array center, i.e., (x_0, y_0, z_0) = (0,0,1.5)m considering Amiet's model coordinate system. The measured noise is shown for the frequencies where the background noise was not dominant, i.e., until approximately 2 kHz. The noise was predicted using Eq. 1, but the results are shown for G_{pp}^{Amiet} (Eq. 2). The results for three different noise predictions are depicted in this figure. For case (1), i.e., $G_{pp}^{Amiet}(\Phi_{ww}^{\mathrm{vK}}(\Lambda_f|_{\mathrm{NTD}}, u_{rms}|_{\mathrm{NTD}}))$, the far-field noise was calculated using the von Kármán spectrum (Eq. 3) with input the turbulence parameters measured at the LE location without the airfoil in the flow, i.e., NTD case. For case (2), i.e., $G_{pp}^{Amiet}(\Phi_{ww}^{\mathrm{RDT}}(\Lambda_f|_{\mathrm{NTD}}, u_{rms}|_{\mathrm{NTD}}))$, the far-field noise was computed using the RDT turbulence spectrum (Eq. 4) with input the turbulence parameters measured at the LE location without the airfoil in the flow, i.e., NTD case. For case (3), i.e., $G_{pp}^{Amiet}(\Phi_{ww}^{\mathrm{RDT}}(\Lambda_f|_{\mathrm{TD}}, u_{rms}|_{\mathrm{TD}}))$, the far-field noise was computed using the RDT turbulence spectrum (Eq. 4) with as input the turbulence parameters measured at the vicinity of the airfoil LE at $x/r_{\mathrm{LE}} = -2$ with the airfoil installed in the test section, i.e., TD case. In short, the noise prediction for case (1) does not account for any turbulence distortion effect. For case (2), the turbulence

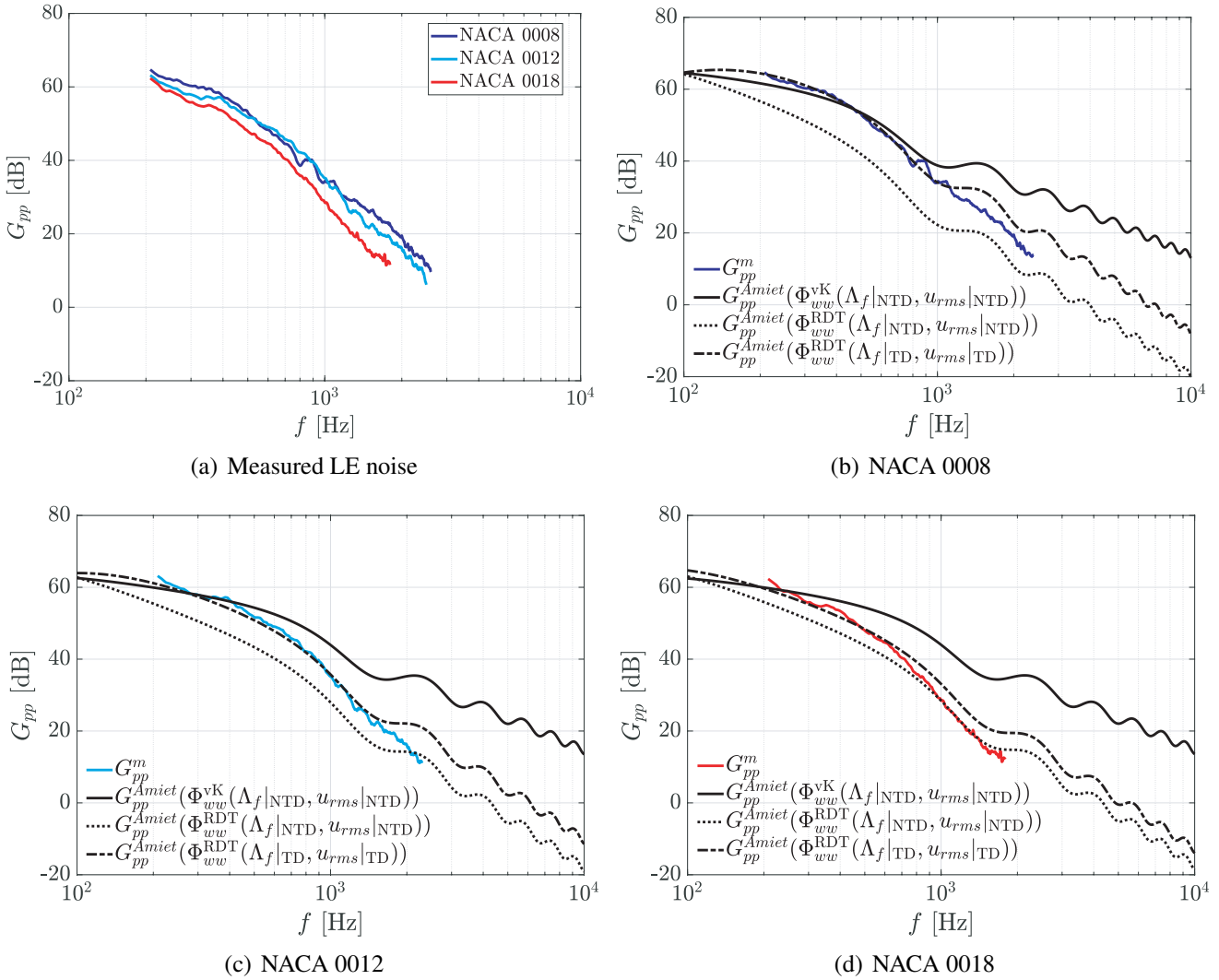

(a) Measured LE noise

(b) NACA 0008

(c) NACA 0012

(d) NACA 0018

Figure 3: PSD of the measured LE far-field noise (G_{pp}^{m}) compared with Amiet's LE noise prediction model (G_{pp}^{Amiet}). Reference pressure for the dB calculation: $p_{\mathrm{ref}} = 20$ µPa.

distortion is taken into account only in the formulation of the turbulence spectrum. For case (3), the turbulence distortion is considered in the turbulence spectrum formulation and in the input values u_{rms} and Λ_f.

Figure 3(a) shows that the LE noise decreases as the thickness and LE radius increase. NACA 0018 has a lower noise level than NACA 0012 for frequencies higher than 300 Hz because the NACA 0018 is thicker and has a larger LE radius than the NACA 0012. The airfoil chord length affects the radiated LE noise, making the comparison between the NACA 0008 with the other airfoils not trivial.

Figures 3(b), 3(c) and 3(d) show that $G_{pp}^{Amiet}(\Phi_{ww}^{\mathrm{vK}}(\Lambda_f|_{\mathrm{NTD}}, u_{rms}|_{\mathrm{NTD}}))$, i.e., the standard Amiet's model, overestimates the LE noise for high frequencies. The noise prediction using the turbulence spectrum based on the RDT, i.e., $G_{pp}^{Amiet}(\Phi_{ww}^{\mathrm{RDT}}(\Lambda_f|_{\mathrm{NTD}}, u_{rms}|_{\mathrm{NTD}}))$, can more accurately predict the noise decay for high frequencies. However, a level difference is still observed between the measured and predicted LE noise. For these two cases, the u_{rms} and Λ_f values used as input for the turbulence spectrum were determined at the airfoil LE position without the airfoil in the flow. However, to accurately model the turbulence spectral energy, independently if the turbulence is distorted or not, the turbulence parameters u_{rms} and Λ_f must be determined at the location of interest. Thus, we believe that the appropriate turbulence input parameters for Φ_{ww}^{RDT} must be determined sufficiently close to the airfoil LE to account for the changes in these parameters caused by the turbulence distortion. Therefore, the noise prediction for case (3), i.e., $G_{pp}^{Amiet}(\Phi_{ww}^{\mathrm{RDT}}(\Lambda_f|_{\mathrm{TD}}, u_{rms}|_{\mathrm{TD}}))$, was computed using Φ_{ww}^{RDT} with u_{rms} and Λ_f values measured at the vicinity of the airfoil LE, i.e., TD case, at $x/r_{\mathrm{LE}} = -2$. A good agreement between the measured and predicted LE noise is achieved for case (3) for frequencies up to 1 kHz. For this case, Amiet's model can predict the noise for low and mid frequencies well. However, the predicted noise deviates from the measurements for high frequencies, mainly for the NACA 0018. These observations are also valid for the other velocity measurements.

5. Conclusions

This paper discusses the turbulence distortion in the vicinity of the airfoil LE caused by different airfoil geometries to understand how the turbulence distortion can be accounted for in Amiet's LE noise prediction model. The turbulence longitudinal length scale and the root-mean-square of the velocity fluctuations decrease as the airfoil LE is approached, which is due to the airfoil blockage effect. Also, Λ_f and u_{rms} at $x/r_{\mathrm{LE}} = -2$ decrease as the airfoil LE radius and thickness decrease. This behavior directly impacts the LE noise generated by these airfoils. The LE noise decreases as the airfoil thickness and LE radius increase, mainly for high frequencies. The standard Amiet's noise prediction model overestimates the LE noise for high frequencies. The noise prediction for these frequencies improves by using the turbulence spectrum based on the RDT; however, the noise level does not match well with the measurements in the entire frequency range. Hence, just using the RDT-based turbulence spectrum is not enough to obtain an accurate noise prediction. A good agreement between the measured and predicted LE noise is achieved when the RDT-based turbulence spectrum is used with input the u_{rms} and Λ_f values measured at the vicinity of the airfoil LE, i.e., $x/r_{\mathrm{LE}} = -2$. The turbulence parameters u_{rms} and Λ_f in the proximity of the airfoil LE can be determined from experiments or simulations, and it can be estimated by using the formulation proposed by dos Santos et al. [10, Eq. 12] for a NACA 0008.

The main contribution of this research was to show that the turbulence distortion can be accounted for in Amiet's LE noise prediction for different airfoil geometries. This is achieved by using as input to the model: (1) the RDT-based turbulence spectrum and (2) the turbulence parameters u_{rms} and Λ_f in the proximity of the airfoil LE. These inputs result in an accurate noise prediction for low and mid frequencies and an improved prediction for high frequencies for airfoils with thickness up to 18% of the chord length.

REFERENCES

1. Amiet, R. Noise due to turbulent flow past a trailing edge, *Journal of Sound and Vibration*, **47** (3), 387 – 393, (1976).

2. Glegg, S. and Devenport, W., *Aeroacoustics of Low Mach Number Flows*, Academic Press, London, United Kingdom, 185–345 (2017).

3. Amiet, R. Acoustic radiation from an airfoil in a turbulent stream, *Journal of Sound and Vibration*, **41** (4), 407 – 420, (1975).

4. Devenport, W. J., Staubs, J. K. and Glegg, S. A. Sound radiation from real airfoils in turbulence, *Journal of Sound and Vibration*, **329** (17), 3470–3483, (2010).

5. Moreau, S. and Roger, M. Effect of angle of attack and airfoil shape on turbulence-interaction noise, *11^{th} AIAA/CEAS Aeroacoustics Conference*, (2005).

6. Oerlemans, S. and Migliore, P. Aeroacoustic wind tunnel tests of wind turbine airfoils, *10^{th} AIAA/CEAS Aeroacoustics Conference*, (2004).

7. Gill, J., Zhang, X. and Joseph, P. Symmetric airfoil geometry effects on leading edge noise, *The Journal of the Acoustical Society of America*, **134** (4), 2669–2680, (2013).

8. Hunt, J. C. R. A theory of turbulent flow round two-dimensional bluff bodies, *Journal of Fluid Mechanics*, **61** (4), 625–706, (1973).

9. Santana, L. D., Christophe, J., Schram, C. and Desmet, W. A rapid distortion theory modified turbulence spectra for semi-analytical airfoil noise prediction, *Journal of Sound and Vibration*, **383**, 349–363, (2016).

10. dos Santos, F. L., Botero-Bolivar, L., Venner, C. H. and de Santana, L. Inflow turbulence distortion for airfoil leading-edge noise prediction, 28^{th} AIAA/CEAS Aeroacoustics Conference, (2022).

11. de Santana, L., Sanders, M. P. and Venner, C. H. The utwente aeroacoustic wind tunnel upgrade, *2018 AIAA/CEAS Aeroacoustics Conference*, AIAA 2018-3136, (2018).

12. von Heesen, W. and Höpfer, M. Suppression of wind tunnel buffeting by active flow control, *SAE 2004 World Congress & Exhibition*, (2004).

13. Brooks, T. and Humphreys, W. Effect of directional array size on the measurement of airframe noise components, *5^{th} AIAA Aeroacoustics Conference*, (1999).

14. Hinze, J. O., *Turbulence*, McGraw-Hill, New York, USA, 4–44 (1975).

15. Mish, P. F. and Devenport, W. J. An experimental investigation of unsteady surface pressure on an airfoil in turbulence—part 2: Sources and prediction of mean loading effects, *Journal of Sound and Vibration*, **296** (3), 447–460, (2006).

16. dos Santos, F. L., Botero-Bolivar, L., Venner, C. and de Santana, L. D. Modeling the turbulence spectrum dissipation range for leading edge noise prediction, *AIAA Journal*, (2022).

17. de Santana, L., *Semi-analytical methodologies for airfoil noise prediction*, Ph.D. thesis, KU Leuven, (2015).